ROYAL SOCIETY
OF CHEMISTRY

PAPER

Check for updates

Redox mechanism by lattice sulphur in an Fe-based catalyst for propane dehydrogenation with H_2S co-feeding†

Ryo Watanabe, [ID] *[a] Priyanka Verma, [ID] [b] Hiroshi Akama[a] and Choji Fukuhara*[a]

Iron-based catalysts supported on SiO_2 (Fe/SiO_2) exhibit unique resistance to sulphur poisoning and sustained activity for propane dehydrogenation (PDH) under hydrogen sulfide (H_2S) co-feeding. In this study, noble metals (Pd, Pt, Ru) were incorporated to enhance catalytic performance, among which Ru significantly improved both activity and durability. Transient pulse experiments coupled with mass spectrometry revealed that the PDH reaction proceeds *via* a regenerable redox mechanism involving lattice sulphur (S^{2-}), where Ru promotes both the release and re-incorporation of S^{2-} species. Spectroscopic analysis using XPS and Ru K-edge EXAFS showed that Ru exists in both metallic and sulphidic forms, and that interfacial electron transfer from Fe to Ru increases the Fe oxidation state. DFT calculations based on a Ru−FeS interface confirmed this electron redistribution and identified balanced activation barriers for key steps such as C−H activation (81.3 kJ mol^{-1}) and S^{2-} regeneration (80.8 kJ mol^{-1}). The synergy between structural characterization and theoretical modelling supports a robust and reversible lattice-sulphur-mediated catalytic cycle. These findings establish Ru−Fe/SiO$_2$ as a promising redox catalyst for selective PDH under H_2S-rich conditions, and demonstrate a viable strategy for utilizing sulfur-containing streams in alkane upgrading.

Sustainability spotlight

Hydrogen sulfide (H_2S), a hazardous byproduct of fossil fuel refining, is typically treated as waste despite its high sulfur content. This work transforms H_2S from a pollutant into a reactive component in a circular catalytic process for propane dehydrogenation, using earth-abundant Fe-based catalysts. The redox cycle of lattice sulfur enables coke-resistant, regenerable dehydrogenation with minimal environmental impact. This strategy directly addresses waste valorization, resource efficiency, and cleaner chemical production. It aligns with the UN sustainable development goals: goal 12 (responsible consumption and production), goal 13 (climate action), and goal 9 (industry, innovation and infrastructure), by integrating waste reuse with sustainable catalysis for light-alkane upgrading.

1. Introduction

The sustainable transformation of small alkanes into valuable olefins using circular and waste-derived inputs is increasingly central to achieving low-carbon chemical manufacturing. Among light olefins, propylene plays a pivotal role as a feed-stock for polypropylene, acrylonitrile, propylene oxide, and other essential industrial chemicals. With growing global demand, the limitations of conventional processes such as steam cracking and fluid catalytic cracking (FCC)—including poor selectivity, rigid feedstock requirements, and high energy intensity—have become more apparent.[1–3] As a result, on-

purpose technologies such as propane dehydrogenation (PDH) have gained momentum for converting abundant, low-cost propane, particularly from shale gas, into high-purity propylene.

Platinum- and chromium-based catalysts have traditionally been used in commercial PDH processes.[4–6] However, these systems suffer from rapid deactivation due to coke deposition, requiring oxidative regeneration at high temperatures that induces irreversible sintering and phase transformations.[7–10] Consequently, the development of coke-resistant, regenerable, and thermally stable catalysts is essential to improving the durability and efficiency of PDH technology.

To this end, several catalytic systems based on oxides of vanadium, gallium, indium, tungsten, and iron have been studied as alternatives.[11–17] These materials often exploit redox activity or tailored surface acidity to promote C−H activation while suppressing coke formation. Iron-based catalysts are particularly attractive due to their earth abundance, low toxicity, and tunable redox behaviour. In parallel, sulphur-containing

[a]Department of Applied Chemistry and Biochemical Engineering, Graduate School of Engineering, Shizuoka University, 3-5-1 Johoku, Chuo-ku, Hamamatsu, Shizuoka 432-8561, Japan. E-mail: watanabe.ryo@shizuoka.ac.jp

[b]Department of Chemistry, Indian Institute of Technology Delhi, Hauz Khas, New Delhi, 110016, India

catalysts—especially metal sulphides—have gained attention for their unique ability to activate alkanes *via* lattice sulphur species. Unlike metallic catalysts, metal sulphides can operate through redox cycles involving lattice S^{2-}, enabling oxidative dehydrogenation (ODH)-like behaviour without external oxidants, and offering intrinsic resistance to coking.[18–20]

Wang and co-workers reported that metal sulphide catalysts exhibit high initial activity for isobutane dehydrogenation, though rapid deactivation occurs due to sulphur depletion under reducing conditions.[21] To overcome this, Arinaga *et al.* proposed a redox-type ODH mechanism using lattice S^{2-} and elemental disulphur (S_2) as a soft oxidant.[22] While this strategy allows sulphur cycling, it still relies on external oxidants and does not fully address sulphur loss during reaction.

Hydrogen sulphide (H_2S), a major byproduct of hydrodesulphurisation and natural gas processing, presents a critical opportunity in this context. While it is conventionally treated *via* the Claus process to yield elemental sulphur, the global sulphur supply already exceeds industrial demand by several million metric tons per year, leading to large-scale accumulation of sulphur waste.[23] From the standpoint of sustainable resource management, redefining H_2S from a waste to a reactive feedstock can provide not only a route to mitigate environmental burden but also a pathway to enable novel circular catalytic processes based on sulphur redox chemistry.

In our previous studies,[24,25] we demonstrated that silica-supported transition metal catalysts—particularly Fe/SiO₂—can perform PDH in the presence of H_2S by leveraging lattice sulphur species as reactive oxygen surrogates. These systems showed stable activity and high propylene selectivity, especially for heavier alkanes such as butane and pentane, suggesting the existence of a lattice S^{2-}-based redox cycle. However, these studies were predominantly phenomenological and did not address the atomic structure of the active sites, the mechanism of sulphur release and regeneration, or the role of co-fed H_2S in sustaining catalytic function.

The present work advances this concept significantly by introducing ruthenium (Ru) as a redox promoter in Fe/SiO₂-based catalysts. We hypothesize that Ru facilitates lattice sulphur mobility and enhances the rate of S^{2-} release and re-sulphidation, thereby improving catalytic stability and turnover. To validate this, we employ a combination of transient pulse experiments, surface and bulk kinetic modeling, and density functional theory (DFT) calculations using the nudged elastic band (NEB) method. These methods allow us to quantify the dynamics of S^{2-} consumption and regeneration, evaluate the energetic feasibility of each elementary step, and uncover the synergistic electronic interactions between Fe and Ru that accelerate sulphur redox cycling.

By establishing a mechanistic and kinetic framework for lattice S^{2-}-mediated propane dehydrogenation using H_2S as an *in situ* oxidant, this work offers a new strategy for sustainable alkane upgrading. The system not only valorises H_2S but also achieves high PDH activity and stability under sulphur-rich conditions, a domain where conventional metal catalysts typically fail due to sulphur poisoning. This study thus exemplifies a circular sulphur chemistry approach—redefining waste H_2S as

a functional oxidant—and contributes a robust design concept for sulphur-tolerant, regenerable dehydrogenation catalysts compatible with future low-waste, low-carbon chemical processing.

2. Experimental

2.1 Preparation and characterisation of the catalyst

The Fe/SiO₂ catalysts were prepared using an impregnation method. The SiO₂ support (JRC-SIO-4) was obtained from the Catalysis Society of Japan. The support was immersed in distilled water for 6 h, followed by the addition of iron(III) nitrate nonahydrate, and the mixture was stirred for another 2 h. The resulting slurry was dried at 80 °C and then calcined at 500 °C for 1 h. For the preparation of bimetallic catalysts, noble metal precursors (Ru, Pt, or Pd) were co-impregnated with the Fe precursor onto the SiO₂ support. In all cases, the Fe loading was fixed at 10 wt%. For initial catalyst screening (Fig. 1(a)), the molar ratio of noble metal to Fe was set to 0.2 (*i.e.*, Fe : M = 5 : 1), and this ratio was applied consistently for all comparisons across different noble metals. Among the noble metals tested, Ru exhibited the most pronounced promotional effect on catalytic activity and stability. Therefore, the Fe/Ru molar ratio was further varied over a wide range (Fe/Ru = 1/8 to 8) to optimise the bimetallic composition. The catalyst precursors were dried and calcined under the same conditions as the monometallic Fe/SiO₂ catalyst.

2.2 Evaluation of catalytic performance

The PDH performance of the prepared catalysts, including their catalytic activity, product selectivity, and stability, was evaluated using a conventional fixed-bed reactor. The reaction was carried out at 600 °C under atmospheric pressure. Propane was fed into the catalyst bed with H_2S co-feeding balanced by helium. The molar ratio of H_2S to propane was 0.25 to 2.0. The propane feed rate was 2.5 mL min⁻¹ (SATP), and the catalyst weight was 0.25 g. The gaseous reactants and products in the effluent gases (*i.e.*, C_3H_8, CH_4, C_2H_4, and C_3H_6) were collected using a micro-syringe and then injected into an offline thermal conductivity detector gas chromatograph and a flame ionisation detector gas chromatograph (GC-8A; Shimadzu Inc., Japan). Propane conversion ($X_{C_3H_8}$) and product selectivity (Sel) were calculated using the following equations:

$$X_{C_3H_8} = (F_{CH_4} + 2 \times F_{C_2H_4} + 3 \times F_{C_3H_6})/(3 \times F_{C_3H_8}) \times 100 \quad (1)$$

$$\text{Sel} = (N \times F_i)/(F_{CH_4} + 2 \times F_{C_2H_4} + 3 \times F_{C_3H_6}) \times 100 \quad (2)$$

where F_i is the flow rate of the reactant and products, and N is the number of carbon atoms in the product.

2.3 Characterisation of catalysts

The amount of carbon deposited on the catalyst after the reaction was measured using an elemental analyser (Flash EA 1112, Thermo Fisher Electron Inc., USA). The catalyst sample (1.5 mg) was placed in an aluminium foil cup for measurement. The
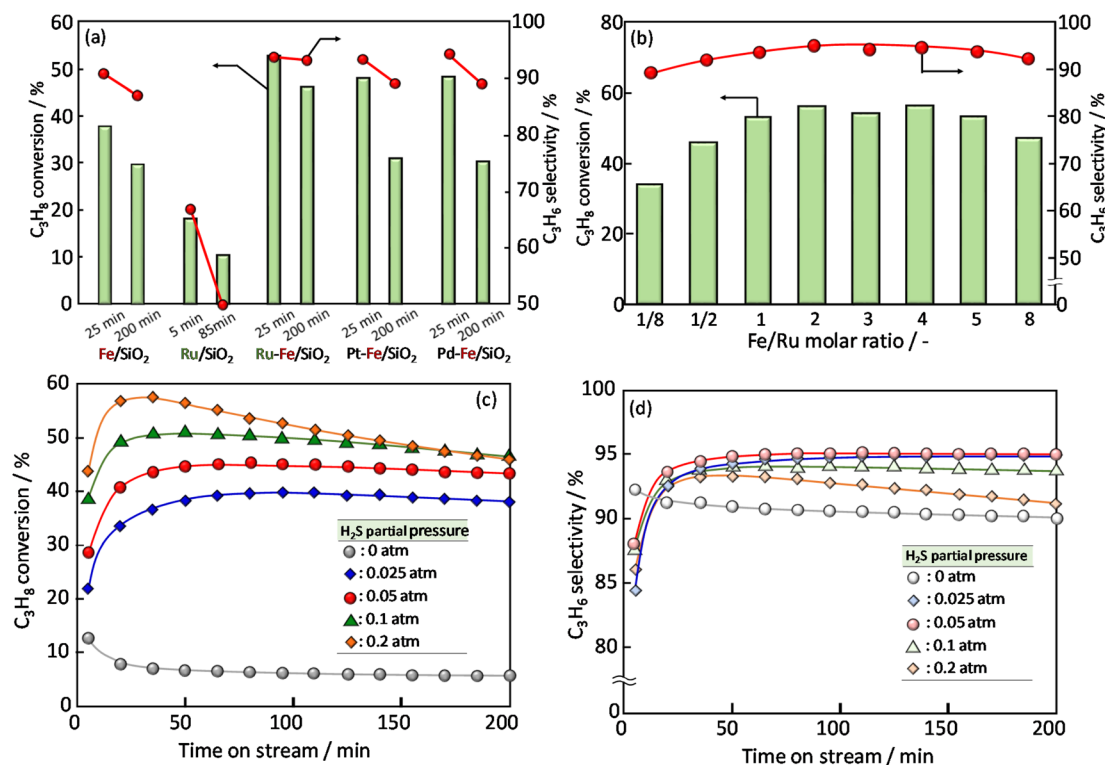
Fig. 1 (a) Effect of noble metal (Ru, Pt, Pd) loading onto Fe/SiO$_2$ for propane dehydrogenation with H$_2$S co-feeding. (b) Optimum ratio of Fe to Ru in Ru–Fe/SiO$_2$ catalyst. (c) Propane conversion and (d) propylene selectivity over Ru–Fe/SiO$_2$ catalyst under various H$_2$S partial pressures.

amount of carbon deposition on the catalyst was determined by increasing the temperature from room temperature to 900 °C. The amount of coke formed was calculated from the CO$_x$ produced and detected using the GC-FID methaniser.

The crystal structure of the prepared catalyst was characterised by XRD analysis using CuKα radiation (λ = 1.54 Å, Ultima IV; Rigaku Inc., Japan).

The electronic structures of the catalyst surface elements were determined using X-ray photoelectron spectroscopy (XPS). We analysed all the obtained spectra by fitting them with a Gaussian function and used Si 2p as the reference for the energy calibration of the XPS spectra, setting the peak top of the combined wave of Si 2p$_{1/2}$ and Si 2p$_{3/2}$ at 103.6 eV.

The Ru K-edge extended X-ray absorption fine structure (EXAFS) measurements were conducted at the Aichi Synchrotron Radiation Center (Beamline BL5S1, Aichi Science & Technology Foundation, Japan). The spectra were acquired in transmission mode using a Si(111) double-crystal monochromator at room temperature. The energy was calibrated with a Ru foil standard. The samples were pressed into self-supporting pellets and sealed in an inert atmosphere to prevent oxidation prior to measurement. Multiple scans were averaged to improve the signal-to-noise ratio. EXAFS data processing, including background subtraction, normalization, and Fourier transformation, was carried out using the Athena and Artemis software packages. The structural fitting was performed in R-space using theoretical phase and amplitude functions generated by FEFF. Coordination numbers, bond distances, and

Debye–Waller factors were refined to obtain local structural parameters around Ru atoms.

2.4 Analysis of the reaction mechanism

The reaction mechanism was analysed by transient response experiments as follows: First, propane and H$_2$S were fed to the catalyst bed at 600 °C. After reaching a steady state, the surface-adsorbed species were purged and desorbed by He flow. Subsequently, propane or H$_2$S was fed into the catalyst bed separately. The reaction conditions were as follows: reaction temperature: 600 °C; catalyst amount: 100 mg; propane flow rate: 2 ml min^{-1}; H$_2$S flow rate: 1 min^{-1}; internal standard gas (Ar): 5 ml min^{-1}; total flow rate of 100 ml min^{-1}, balanced with He. Temporal changes in the reactants and products were monitored using a quadrupole mass spectrometer (QMS) connected to the reactor outlet. The QMS monitored the signals for five key fragments at m/z 2 (H$_2$), 20 (Ar), 29 (propane), 34 (H$_2$S), and 41 (propylene).

2.5 Density functional theory calculation

The reaction barrier was estimated through nudged elastic band (NEB) calculations, which were carried out by assuming well-defined initial and final states along the reaction pathway. These calculations were conducted using a combination of quantum ESPRESSO and advance/NanoLabo, both of which are widely used platforms for first-principles simulations. The computational framework employed the pseudopotential

method based on plane-wave basis functions, and the generalized gradient approximation with the Perdew–Burke–Ernzerhof (GGA-PBE) functional was adopted as the exchange–correlation approximation. Key computational parameters, including the cutoff energies for the wave function and charge density, as well as the density and mesh of the k-point sampling in reciprocal space, were carefully optimized to ensure numerical convergence and accuracy. Detailed conditions and parameter settings used in the calculations for each dataset are presented in the corresponding sections.

3. Results and discussion

3.1 Effect of promoter (Pt, Pd, Ru) addition to the Fe/SiO$_2$ catalyst

To improve the dehydrogenation performance of the Fe/SiO$_2$ catalyst under H$_2$S co-feeding conditions, noble metals—Pd, Pt, and Ru—were introduced. As shown in Fig. 1(a), the addition of these metals significantly enhanced both propane conversion and propylene selectivity compared to the unmodified Fe/SiO$_2$ catalyst. Among them, the Ru-modified catalyst (Ru–Fe/SiO$_2$) exhibited the most pronounced promotional effect, indicating that Ru plays a particularly effective role in enhancing the redox functionality of the catalytic system under sulphidic conditions. In contrast, the Ru/SiO$_2$ catalyst lacking Fe showed minimal activity, underscoring the essential role of Fe in forming the redox-active sulphide phase.

The superior performance of Ru relative to Pt and Pd is attributed to differences in their redox properties and sulphidation behavior. Ru is known to readily form sulphide phases such as RuS$_2$ under H$_2$S exposure. However, its electronic structure allows it to maintain partial metallic character under reducing or reactive environments. This redox flexibility enables Ru to promote both the release and regeneration of lattice sulphur species in adjacent Fe sites, thereby facilitating the redox cycle. In contrast, Pd and Pt tend to form more stable and less redox-active sulphides that may suppress dynamic sulphur turnover, resulting in lower catalytic enhancement.

To further explore the synergistic effect between Fe and Ru, the Fe/Ru molar ratio was systematically varied from 1/8 to 8, as shown in Fig. 1(b). The results reveal a volcano-type dependence of both conversion and selectivity on the Fe/Ru ratio, with optimum performance observed at ratios between 2 and 4. When the Ru content was too high, the excessive surface coverage and deeper sulphidation likely suppressed the redox function of Fe. Conversely, insufficient Ru loading limited the promotion of lattice sulphur dynamics. These findings emphasize the importance of balancing the redox-active Fe phase with an appropriate amount of Ru promoter to achieve optimal catalytic performance.

Fig. 1(c) and (d) illustrate the effect of H$_2$S partial pressure on propane conversion and propylene selectivity. In the absence of H$_2$S, the catalyst deactivated rapidly, confirming that lattice sulphur species are consumed during the reaction and must be externally replenished. The introduction of H$_2$S restored and stabilized the catalytic activity, even at low partial pressures, indicating its essential role in maintaining the redox cycle. The

presence of an induction period upon H$_2$S introduction suggests a gradual build-up of lattice sulphur within the catalyst structure. As the H$_2$S partial pressure increased, both conversion and selectivity improved and then plateaued, indicating a positive reaction order with respect to H$_2$S. These results support a redox-type mechanism in which lattice S^{2-} serves as a soft oxidant for C–H activation and is subsequently replenished by H$_2$S through re-sulphidation. Ru likely facilitates both sulphur release and reincorporation by modulating the interfacial redox environment between the metal and the sulphide lattice.

While the data shown in Fig. 1 represent relatively short-term reaction behavior, the Ru–Fe/SiO$_2$ catalyst maintained high activity and selectivity over several hours without significant deactivation. Extended reaction tests reported elsewhere demonstrated that the co-feeding of H$_2$ further improved catalyst durability, particularly under H$_2$S-rich conditions.[26] This stabilizing effect is especially evident in Ru-containing systems and is believed to originate from the ability of H$_2$ to suppress the irreversible formation of fully sulphidized Ru phases such as RuS$_2$. By maintaining Ru in a partially metallic state, H$_2$ co-feeding allows the Ru–Fe interface to retain redox flexibility, thereby enhancing lattice sulphur turnover and sustaining the catalytic cycle.

Taken together, these findings demonstrate that Ru–Fe/SiO$_2$ enables an efficient and regenerable redox cycle for PDH under H$_2$S co-feeding, and that the redox capability of the noble metal plays a critical role in modulating sulphur dynamics. By leveraging the redox-tolerant nature of Ru and the redox-active lattice of FeS$_x$, this system offers a promising design for sulphur-tolerant, coke-resistant PDH catalysts capable of utilizing H$_2$S as a functional reactant.

3.2 Reaction mechanism of the Fe-based catalyst

To directly verify the proposed redox mechanism involving lattice sulphur species in Fe-based catalysts under H$_2$S co-feeding conditions, a series of cyclic pulse experiments was performed using Fe/SiO$_2$ and Ru–Fe/SiO$_2$ catalysts. This approach enabled the real-time tracking of gas-phase products in response to controlled switching of reactant gases and provided direct experimental evidence—reported here for the first time—that lattice S^{2-} can actively participate in propane dehydrogenation and be replenished via H$_2$S in a reversible redox cycle. The observed product distributions not only confirmed the fundamental role of lattice sulphur but also uncovered distinct kinetic differences between Fe-only and Ru-promoted catalysts, which were further examined through kinetic modeling.

Fig. 2(a) shows the time-resolved product distribution over Fe/SiO$_2$ under a five-step cyclic pulse protocol designed to disentangle sulphur consumption and regeneration steps:

Operation (1): the catalyst was first exposed to a mixture of C$_3$H$_8$ and H$_2$S until steady-state conversion was achieved.

Operation (2): upon switching to pure propane, both C$_3$H$_6$ and H$_2$S were immediately observed in near-stoichiometric quantities, strongly supporting the occurrence of oxidative
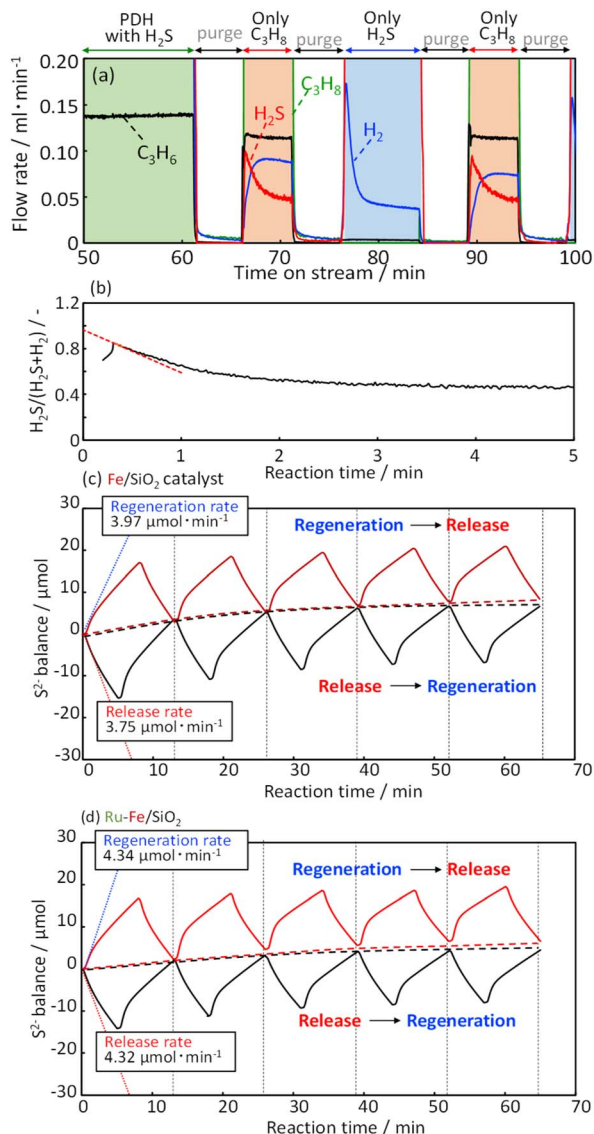
Fig. 2 (a) Temporal change of flow rate in the periodic pulse experiment over the Fe/SiO$_2$ catalyst. (b) Ratio of H$_2$S/(H$_2$S + H$_2$) with reaction time. S^{2-} balance in (c) Fe/SiO$_2$ and (d) Ru–Fe/SiO$_2$ catalysts calculated by H$_2$S production in S^{2-} release and H$_2$ production in S^{2-} regeneration.

dehydrogenation via lattice S^{2-} (C$_3$H$_8$ + S^{2-} → C$_3$H$_6$ + H$_2$S + V$_S$), and providing direct chemical evidence that lattice sulphur atoms are transferred to the product phase.

Operation (3): after purging, H$_2$S alone was introduced. A distinct evolution of H$_2$ was detected, consistent with the refilling of sulphur vacancies by H$_2$S (H$_2$S + V$_S$ → S^{2-} + H$_2$), demonstrating that the lattice redox site is chemically reactivated via H$_2$S dissociation.

Operation (4): switching back to propane again yielded simultaneous formation of C$_3$H$_6$ and H$_2$S, confirming that the regenerated sulphur site re-engaged in dehydrogenation.

Operation (5): final exposure to H$_2$S restored the initial redox state, completing the cycle.

These cyclic gas-switching experiments offer the first direct, time-resolved evidence that lattice sulphur atoms function as

redox shuttles, repeatedly consumed and reconstituted through chemically reversible steps. The close temporal alignment of H$_2$S and H$_2$ signals with gas switching transitions demonstrates that these transformations are not incidental but are causally linked to the state of the lattice S^{2-}. This validates the proposed redox loop and establishes a mechanistic role for sulphur vacancies in the catalytic cycle.

To assess the dynamic redox state of the catalyst surface prior to and during reaction onset, the time-resolved H$_2$S/(H$_2$S + H$_2$) ratio was analyzed, as shown in Fig. 2(b). This ratio represents the fraction of sulphur-derived products that appear as H$_2$S versus H$_2$ immediately after switching the feed to propane, and provides insight into the instantaneous surface chemistry. At the moment of switching, the extrapolated H$_2$S/(H$_2$S + H$_2$) ratio approaches unity, indicating that the initial product is almost exclusively H$_2$S. This implies that the catalyst surface, under steady-state C$_3$H$_8$–H$_2$S co-feeding, is saturated with lattice sulphur species capable of releasing H$_2$S via oxidative dehydrogenation. In other words, a reactive surface state enriched in S^{2-} is pre-formed during the co-feeding period. As the reaction proceeds and lattice sulphur is gradually consumed by the dehydrogenation reaction (C$_3$H$_8$ + S^{2-} → C$_3$H$_6$ + H$_2$S + V$_S$), the H$_2$S/(H$_2$S + H$_2$) ratio decreases and H$_2$ production becomes more dominant. This temporal shift reflects a mechanistic transition: initially, the redox pathway involving lattice S^{2-} dominates, but as surface sulphur is depleted, non-redox Langmuir–Hinshelwood-type dehydrogenation pathways (which generate H$_2$ directly) begin to prevail. Thus, the observed time-dependence of the product ratio is not merely a kinetic artifact but serves as a sensitive probe of the evolving surface state and mechanistic switching. This analysis underscores that the catalyst does not maintain a constant redox character throughout reaction, and that its activity is governed by the availability and renewal of lattice sulphur at the surface.

To further evaluate the redox reversibility and quantify the extent of lattice sulphur cycling, the cumulative amounts of sulphur-containing species evolved during each half-cycle were analyzed and are presented in Fig. 2(c) and (d). In these experiments, two different initial conditions were adopted: (i) starting from a steady-state redox-active surface prepared by C$_3$H$_8$–H$_2$S co-feeding, followed by switching to propane only; and (ii) beginning with a surface regenerated by H$_2$S exposure, followed by propane feeding. In both cases, the evolved amounts of H$_2$S and H$_2$ were integrated over time and plotted as functions of reaction cycle, assuming that all detected sulphur originates from lattice S^{2-}. The resulting profiles exhibit repeated and quantitatively consistent evolution and re-incorporation of sulphur species, indicating that the redox process proceeds in a cyclic and reproducible fashion. Quantitative analysis of the initial slopes of the H$_2$S and H$_2$ evolution curves further supports this interpretation. As shown in Fig. 2(c) and (d), Fe/SiO$_2$ exhibited sulphur release and regeneration rates of 3.75 and 3.97 µmol min^{-1}, respectively, while Ru–Fe/SiO$_2$ showed higher rates of 4.32 and 4.34 µmol min^{-1}. These values confirm that the incorporation of Ru accelerates both forward (oxidative) and reverse (reductive) components of the sulphur redox cycle. The combination of cumulative integration and initial rate

analysis clearly demonstrates that the lattice sulphur cycle is both chemically reversible and kinetically active, with Ru enhancing the rate of lattice S^{2-} turnover. This observation provides compelling evidence that the Fe-based catalysts undergo genuine redox cycling, wherein lattice sulphur atoms migrate in and out of the active surface zone in synchrony with the external gas environment. Taken together with the findings from Fig. 2(b), these data demonstrate that lattice S^{2-} functions as a reversible redox mediator: it is first consumed during oxidative dehydrogenation and subsequently replenished *via* H_2S, completing a closed catalytic loop. This behavior confirms that the observed activity is not attributable to irreversible sulphur loss or surface contamination, but to a dynamic redox exchange process that repeatedly mobilizes lattice sulphur under realistic operating conditions.

To clarify the kinetic origin of these trends, we applied a surface-plus-bulk reaction model to fit the experimental sulphur release and regeneration profiles. The model assumes two distinct lattice sulphur domains: surface-accessible sulphur (Q_{surf}) with a fast rate constant k_1, and bulk sulphur (Q_{bulk}) with a slower diffusion-limited rate constant k_2. The following equation describes the cumulative amount of sulphur consumed or replenished over time t:

$$S(t) = Q_{surf} \times (1 - \exp(-k_1 \cdot t)) + Q_{bulk} \times (1 - \exp(-k_2 \cdot t)) \quad (3)$$

The bulk sulphur capacity Q_{bulk} was fixed at 125 μmol, based on total Fe content and assuming full sulphidation. The bulk rate constant k_2 was shared between release and regeneration processes to isolate the surface kinetic contribution.

The fitting results were directly included in the main text and are shown in Fig. S1 in ESI data.† For Fe/SiO$_2$, the lattice sulphur release process was characterized by $Q_{surf} = 7.01$ μmol and $k_1 = 0.435$ min^{-1}, while the regeneration step yielded $Q_{surf} = 2.95$ μmol and $k_1 = 1.134$ min^{-1}. These results indicate that sulphur replenishment proceeds more rapidly than its release, likely due to the high reactivity of H_2S toward surface vacancies. The discrepancy in Q_{surf} values also suggests that a fraction of the surface involved in propane activation is not immediately accessible for re-sulphidation, possibly reflecting local site heterogeneity or multistep reoccupation processes.

In Ru–Fe/SiO$_2$, both processes were faster. Sulphur release was characterized by $Q_{surf} = 5.66$ μmol and $k_1 = 0.47$ min^{-1}, while regeneration gave $Q_{surf} = 2.73$ μmol and $k_1 = 1.25$ min^{-1}. These results confirm that Ru enhances the surface reaction kinetics of both redox steps. The total amount of reactive surface sulphur (~10 μmol) was similar between the two catalysts, indicating that Ru improves the redox performance not by increasing active site quantity, but by facilitating sulphur mobility and H_2S activation.

Furthermore, the bulk diffusion constant k_2 remained narrowly distributed (0.014–0.015 min^{-1}) in all fits, confirming that bulk transport is not the rate-limiting factor and validating the model assumption. The surface-controlled dynamics revealed here reinforce the view that enhancing lattice S^{2-} turnover at the gas–solid interface is the key to catalytic improvement.

This quantitative kinetic framework provides the first clear experimental delineation of surface and bulk contributions to lattice sulphur cycling and identifies Ru as a promoter that specifically accelerates the surface exchange steps. The insights gained here can inform rational catalyst design for redox-mediated hydrocarbon conversions, especially those relying on lattice-based activation mechanisms.

To gain molecular-level insight into the redox mechanism underlying propane dehydrogenation (PDH) over Fe-based sulfide catalysts, we performed density functional theory (DFT) calculations using the nudged elastic band (NEB) method to determine the minimum energy pathways and transition states for each elementary step on a model FeS surface. The primary objective of this study was to verify whether lattice S^{2-} species on Fe-based sulfide catalysts can kinetically mediate a reversible redox cycle involving C–H bond activation, sulphur release, and subsequent regeneration *via* H_2S under realistic thermal conditions.

Importantly, Ru was not included in the present DFT model. This decision was deliberate and methodologically necessary: although Ru has been experimentally shown to enhance the kinetics of sulphur redox cycling, the exact atomic-scale structure, distribution, and oxidation state of Ru under reaction conditions remain unresolved. In particular, it is unclear whether Ru is present as isolated atoms, clusters, or in alloyed form with Fe, and whether it directly interacts with lattice S^{2-} or only modifies adjacent electronic environments. Modeling such systems without experimental constraints would introduce uncontrolled uncertainty and potentially obscure the intrinsic behavior of the Fe–S redox system. Therefore, we focused on a pure FeS model to quantitatively evaluate the fundamental energetics of each redox step, providing a clean baseline for interpreting the function of Ru as a promoter in future studies. The FeS(001) surface was selected as the model system for two reasons. First, the relatively low Fe loading in our experimental catalysts (10 wt%) suggests that most exposed Fe species exist as terrace-like domains rather than nanocrystallites or highly defective edges. Second, the (001) facet is widely used in previous theoretical studies of metal sulfides and provides a well-defined platform for assessing surface reaction energetics. Moreover, PDH is generally categorized as a structure-insensitive reaction, meaning that the catalytic trends derived from this surface are expected to be representative. In constructing the mechanistic pathway, we assumed that propane undergoes C–H bond activation directly on Fe sites, with surface hydrogen atoms subsequently migrating across the FeS surface. Given the metallic character of FeS, hydrogen spillover is considered feasible—a phenomenon supported by experimental results showing that atomic hydrogen can migrate from FeS (as well as FeS$_2$ and MoS$_2$) under mild conditions.[27] Once formed, surface H atoms may either recombine to form H$_2$ or react with lattice sulphur to generate H$_2$S, creating a sulphur vacancy (V_S). The final step involves the re-occupation of V_S by dissociative adsorption of H$_2$S, completing the redox cycle.

All relevant adsorption geometries and transition states were optimized using DFT, with NEB employed to evaluate activation barriers. Fig. 3(a) shows the energy profile and atomic structures corresponding to the first and second hydrogen
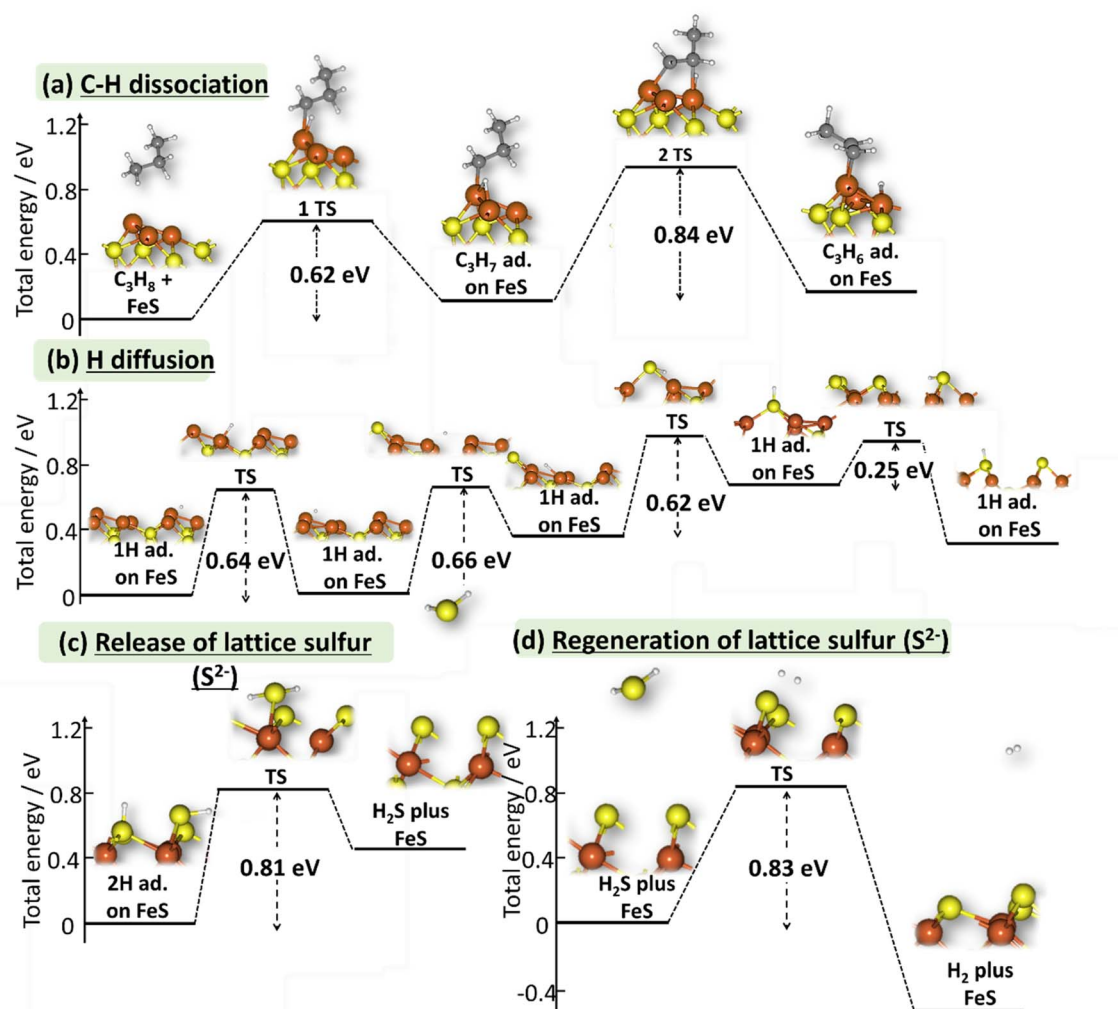
Fig. 3 Activation energy in each step for PDH on an Fe/SiO$_2$ catalyst: (a) C–H dissociation, (b) H diffusion, (c) release of lattice sulfur, and (d) regeneration of lattice sulfur.

abstraction steps from propane. The C–H bond activations proceed with barriers of 0.62 eV and 0.84 eV, respectively, where the latter corresponds to the formation of surface-bound C$_3$H$_6$ and H atoms. These results suggest that propane can be activated on FeS without the need for noble metals, as the barriers are comparable to those on Pt(111). Fig. 3(b) illustrates the pathway for hydrogen migration across the FeS(001) surface. The calculated energy barriers (0.62–0.66 eV) indicate that hydrogen mobility is sufficient to allow for subsequent reactions such as H recombination or interaction with lattice sulphur. In Fig. 3(c), the NEB profile for the release of lattice sulphur is presented. Here, a hydrogen atom reacts with a lattice S^{2-} to form H$_2$S, accompanied by the creation of a sulphur vacancy (V$_S$). The activation energy for this step was calculated to be 0.81 eV. Fig. 3(d) shows the reverse process— lattice sulphur regeneration—where H$_2$S adsorbs and dissociates to fill the sulphur vacancy and release H$_2$. The activation barrier for this step is 0.83 eV, nearly identical to that for sulphur removal. This energetic symmetry strongly supports a fully reversible redox mechanism.

The close correspondence between the energy barriers for S^{2-} removal and reincorporation suggests that lattice sulphur can be both extracted and restored without significant kinetic asymmetry. All key elementary steps—C–H activation, H spillover, S abstraction, and S regeneration—occur within a narrow activation energy window (0.62–0.84 eV), confirming the kinetic accessibility of the full redox cycle. Among these, the second hydrogen abstraction step shows the highest barrier (0.84 eV) and is thus inferred to be rate-determining. Once this step is completed, the downstream redox transformations proceed more readily, in agreement with the sustained catalytic activity observed under reaction conditions. In summary, these DFT calculations validate the mechanistic model proposed from experimental pulse and kinetic data. The results demonstrate that Fe-based sulphide catalysts possess all the necessary attributes to sustain a closed redox cycle involving lattice S^{2-} species, without reliance on prohibitively high activation energies. Although Ru was excluded from this model, the experimentally observed enhancement of sulphur redox kinetics in Ru-containing systems—especially faster H$_2$S activation and

lattice S regeneration—can be interpreted within the same energetic framework. Future calculations incorporating realistic Ru–Fe interfaces based on atomic-scale characterization will be necessary to capture the full promotional effects of Ru. Nevertheless, this study provides the first theoretical quantification of the intrinsic redox capability of FeS surfaces and offers a robust foundation for rational design of lattice-sulphur-mediated redox catalysts.

3.3 Structural and surface property of the Fe/SiO$_2$ catalyst

To elucidate the structural and chemical evolution of the Fe/SiO$_2$ catalyst during propane dehydrogenation (PDH) under H$_2$S co-feeding, we performed time-resolved structural and surface analyses using X-ray diffraction (XRD), X-ray photoelectron spectroscopy (XPS), and bulk elemental analysis. These characterizations aimed to identify the active sulphidic phase, evaluate the thermodynamic and kinetic stability of the catalyst, and understand how lattice sulphur species dynamically participate in the redox cycle under operating conditions.

As shown in Fig. 4(a), the XRD patterns of Fe/SiO$_2$ collected after sulphidation (0 min) and during PDH reaction (up to 145 min) revealed broad features corresponding to amorphous SiO$_2$ and well-defined peaks assignable to Fe$_7$S$_8$ (pyrrhotite), a nonstoichiometric iron sulphide with intrinsic iron vacancies. Notably, no reflections corresponding to metallic Fe or stoichiometric FeS (troilite) were detected at any stage. The peak positions and intensities of Fe$_7$S$_8$ remained unchanged throughout the reaction, indicating that the bulk phase does not undergo structural transformation under reaction conditions. This observation confirms that Fe$_7$S$_8$ is thermodynamically stable in the PDH environment and structurally robust enough to tolerate redox cycling of anionic species without bulk phase degradation.

To evaluate surface chemical changes and redox behavior, XPS measurements were performed at matching time points. The Fe $2p_{3/2}$ spectra (Fig. 4(b)) consistently showed three features: a main peak corresponding to Fe^{2+} in sulphidic coordination, a shoulder attributed to Fe^{3+} from surface oxidation or mixed-valence states, and a broad satellite indicative of high-spin Fe centers. These spectral features remained nearly unchanged during the reaction, both in intensity and binding energy. This invariance suggests that the surface Fe oxidation state distribution is not significantly perturbed during redox cycling, and thus the Fe cations themselves are not the redox-active species in the PDH process.

In contrast, the S 2p spectra (Fig. 4(c)) showed clear evidence of dynamic changes. A strong doublet at binding energies characteristic of lattice S^{2-} was dominant in all spectra, while contributions from oxidized sulphur species (*e.g.*, SO$_x$) were negligible. However, the S^{2-} signal intensity decreased significantly during the initial reaction period and then stabilized at a lower level. This behavior indicates that lattice S^{2-} is extracted during propane activation but is subsequently replenished through dissociative adsorption of H$_2$S, giving rise to a surface-localized redox cycle:
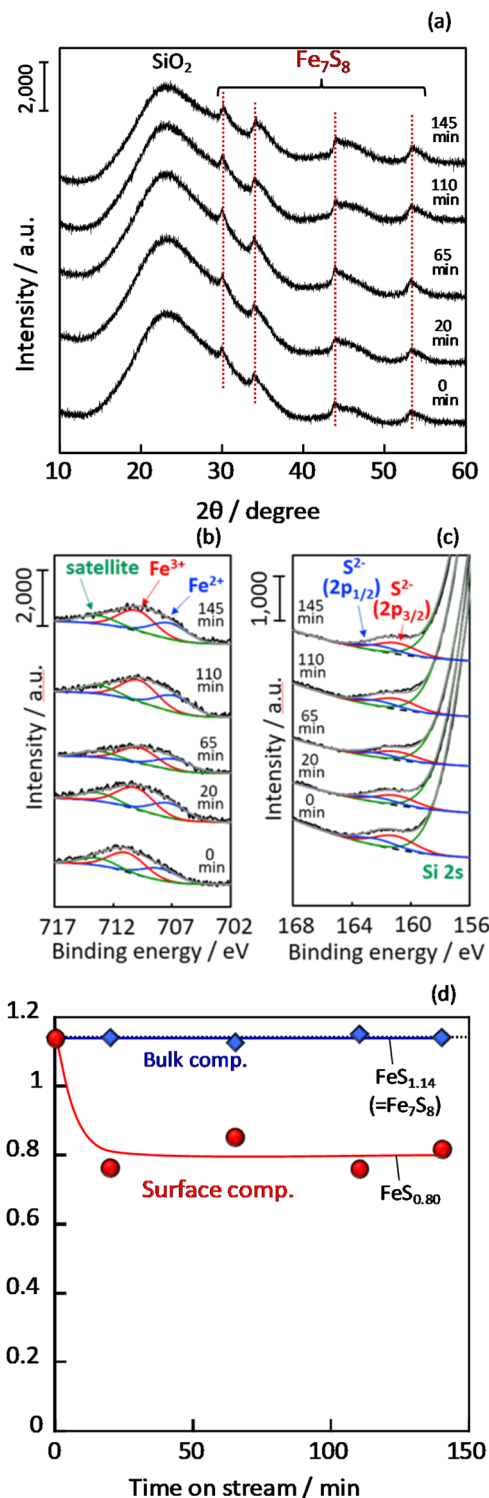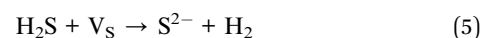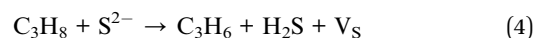

Fig. 4 (a) XRD patterns of the Fe/SiO$_2$ catalyst before and after PDH with H$_2$S co-feeding. XPS spectra of the (b) Fe $2p_{3/2}$ and (c) S 2p of the Fe/SiO$_2$ catalyst. (d) Stoichiometric value x in FeS$_x$ calculated from the elemental analysis result for bulk composition and XPS semi-quantitative value for surface composition.

$$C_3H_8 + S^{2-} \rightarrow C_3H_6 + H_2S + V_S \tag{4}$$

$$H_2S + V_S \rightarrow S^{2-} + H_2 \tag{5}$$

To quantify these changes, we analyzed the FeS_x stoichiometry using both bulk elemental analysis and XPS (Fig. 4(d)). Bulk analysis showed that the S/Fe ratio remained constant at ~1.14 throughout the reaction, consistent with the Fe_7S_8 stoichiometry. In contrast, surface-sensitive XPS revealed a pronounced decrease in the S/Fe ratio from the initial state to a steady value of approximately 0.80. This discrepancy between bulk and surface compositions implies that redox activity—namely S^{2-} removal and reintroduction—is spatially confined to the outermost region of the catalyst particles.

The lack of observable changes in XRD patterns and bulk S/Fe ratio despite significant surface S loss suggests that sulfur exchange occurs predominantly at the particle surface without perturbing the underlying bulk structure. This decoupling is mechanistically significant. Lattice S^{2-} near the surface participates in hydrogen abstraction from propane, creating sulfur vacancies. These vacancies are not rapidly filled by sulfur diffusion from the bulk, likely due to kinetic limitations. Instead, they are reoccupied by dissociatively adsorbed H_2S from the gas phase. As a result, a quasi-steady-state is established in which a thin, surface-active redox layer mediates catalytic turnover while the interior lattice remains compositionally and structurally unaltered.

This surface-localized redox behavior is consistent with the intrinsic properties of Fe_7S_8. As a non-stoichiometric sulphide, Fe_7S_8 contains a high density of iron vacancies and exhibits a layered crystal structure. These features promote defect-mediated diffusion of anions, particularly at elevated temperatures. However, this diffusion is not uniform throughout the crystal; rather, it is energetically favorable near surfaces and interfaces where sulfur vacancies are most abundant. This structural configuration enables efficient lattice sulfur exchange at the surface while preserving the long-range order of the bulk.

Together, these findings establish that Fe_7S_8 functions as a redox host in which catalytic activity is governed by the reversible participation of surface-accessible S^{2-} anions. The maintenance of bulk crystallinity alongside surface redox turnover confirms the catalyst's ability to mediate sulfur-based dehydrogenation without degradation. This mechanistic separation of surface activity from bulk stability is central to the catalyst's performance and durability under H_2S-assisted PDH conditions.

3.4 Role of Ru promoter in Fe/SiO$_2$ catalyst

To elucidate the structural and electronic origin of the superior catalytic performance of Ru–Fe/SiO$_2$ in propane dehydrogenation (PDH) under H_2S co-feeding conditions, we combined extended X-ray absorption fine structure (EXAFS) spectroscopy, X-ray photoelectron spectroscopy (XPS), and density functional theory (DFT) calculations. These complementary analyses were designed to clarify how Ru modifies the active site structure and redox properties of the catalyst, particularly in promoting the lattice sulphur cycle.

Fig. 5 shows the Ru K-edge EXAFS spectra of the Ru–Fe/SiO$_2$ catalyst. The Fourier-transformed EXAFS data exhibit two distinguishable coordination environments around Ru. The first shell, at approximately 2.4 Å, corresponds to Ru–S
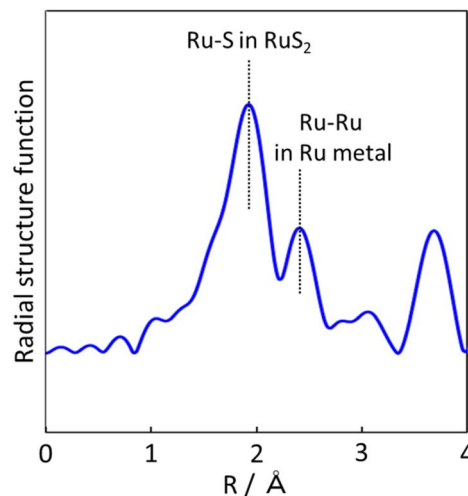

Fig. 5 k^3-Weighted χ (k)-function of extended X-ray absorption fine structure (EXAFS) spectra of the Ru–Fe/SiO$_2$ catalyst.

scattering, indicative of sulphidic Ru species such as RuS$_2$. A second peak at ~2.7 Å, however, is consistent with Ru–Ru metallic bonding, revealing that a significant fraction of Ru exists in the metallic state (Ru^0). This dual coordination environment provides strong structural evidence that both Ru^0 and RuS$_x$ species coexist in the catalyst.

The presence of metallic Ru is particularly important in light of our previous studies, which showed that the introduction of H_2 into the reaction mixture leads to a sustained enhancement in PDH activity over Ru–Fe/SiO$_2$. This behavior strongly suggests that metallic Ru sites contribute directly to C–H activation or hydrogen spillover processes, enabling more efficient dehydrogenation even under sulphidative conditions. In other
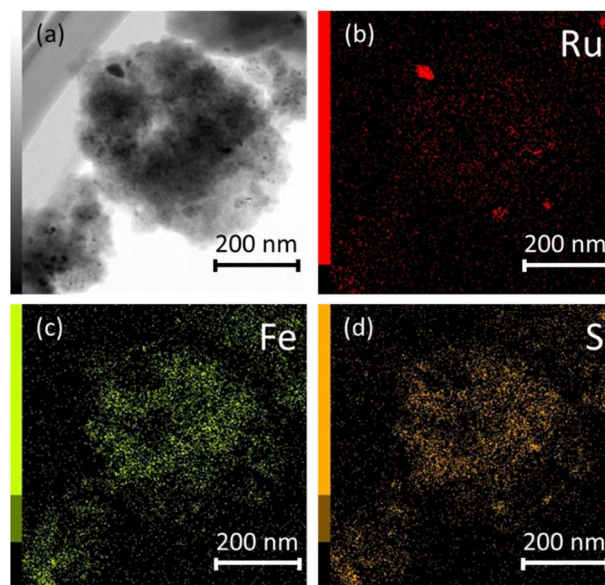

Fig. 6 (a) STEM image and element maps of the (b) ruthenium (Ru), (c) iron (Fe), and (d) sulphur (S) components in the Fe/SiO$_2$ catalyst after PDH with H_2S co-feeding.

words, metallic Ru^0 is considered to promote the redox behaviour of Fe_7S_8, thereby accelerating the release and reincorporation of lattice sulphur. In contrast, sulphidic Ru species such as RuS_2 are likely not involved in the catalytic activity, suggesting that the primary catalytic function of Ru originates from its metallic state. Thus, the presence of metallic Ru at the interface with Fe_7S_8 enhances redox flexibility and contributes to the improved performance of the catalyst.

To further visualize the spatial distribution of Ru, Fe, and S species in the catalyst, STEM-EDX elemental mapping was performed on the sulfided Ru–Fe/SiO2 sample, as shown in Fig. 6. The HAADF-STEM image in Fig. 6(a) reveals aggregated catalyst particles with nanoscale contrast variation. Elemental maps for Ru, Fe, and S are shown in Fig. 6(b)–(d), respectively. Ru is distributed non-uniformly across the catalyst, with certain regions exhibiting strong co-localization with sulfur (Fig. 6(b) and (d)), while other domains show Ru signals with minimal sulfur intensity. This spatial heterogeneity is consistent with the coexistence of multiple Ru species. The sulfur-rich regions are attributed to sulphidic Ru phases such as RuS_2, whereas the sulfur-deficient Ru domains are likely metallic in nature. These results suggest that Ru exists in both sulphidic and metallic forms on the catalyst surface. While the spatial proximity of metallic Ru and FeS domains raises the possibility of interfacial interaction, further evidence is required to evaluate its electronic consequences.

To explore the electronic impact of Ru incorporation, we analyzed the Fe 2p XPS spectra and performed DFT calculations on model Ru–FeS interfaces (Fig. 7). This modeling strategy is further supported by experimental observations that metallic Ru remains catalytically relevant under H_2S-rich conditions. In particular, extended reaction tests have shown that co-feeding H_2 enhances the durability of Ru–Fe/SiO2 catalysts, especially at high H_2S partial pressures.[26] This stabilizing effect is attributed to the suppression of irreversible formation of fully sulphidized Ru phases such as RuS_2. These findings justify our focus on Ru–FeS interfaces rather than RuS_2–FeS configurations, as the active catalytic state is most likely maintained in a partially metallic form under realistic reaction conditions. As shown in Fig. 7(a), the Fe 2p XPS spectra exhibit a clear shift toward higher binding energy in the Ru–Fe/SiO2 catalyst compared to Fe/SiO2, indicating an increase in the average oxidation state of Fe. The Fe^{3+} signal is more prominent in the Ru-containing catalyst, suggesting partial oxidation of Fe through interaction with Ru. This electronic modification remains after high-temperature sulphidation, confirming its intrinsic nature.

To understand the origin of this electronic shift at the atomic level, we constructed a DFT model consisting of metallic Ru clusters in contact with a FeS lattice. As shown in Fig. 7(b), the optimized structure illustrates Ru–Fe interfacial configurations. The layer-resolved electron density analysis (Fig. 7(c) and (d)) indicates that interfacial Fe atoms (Fe_1) transfer electrons to
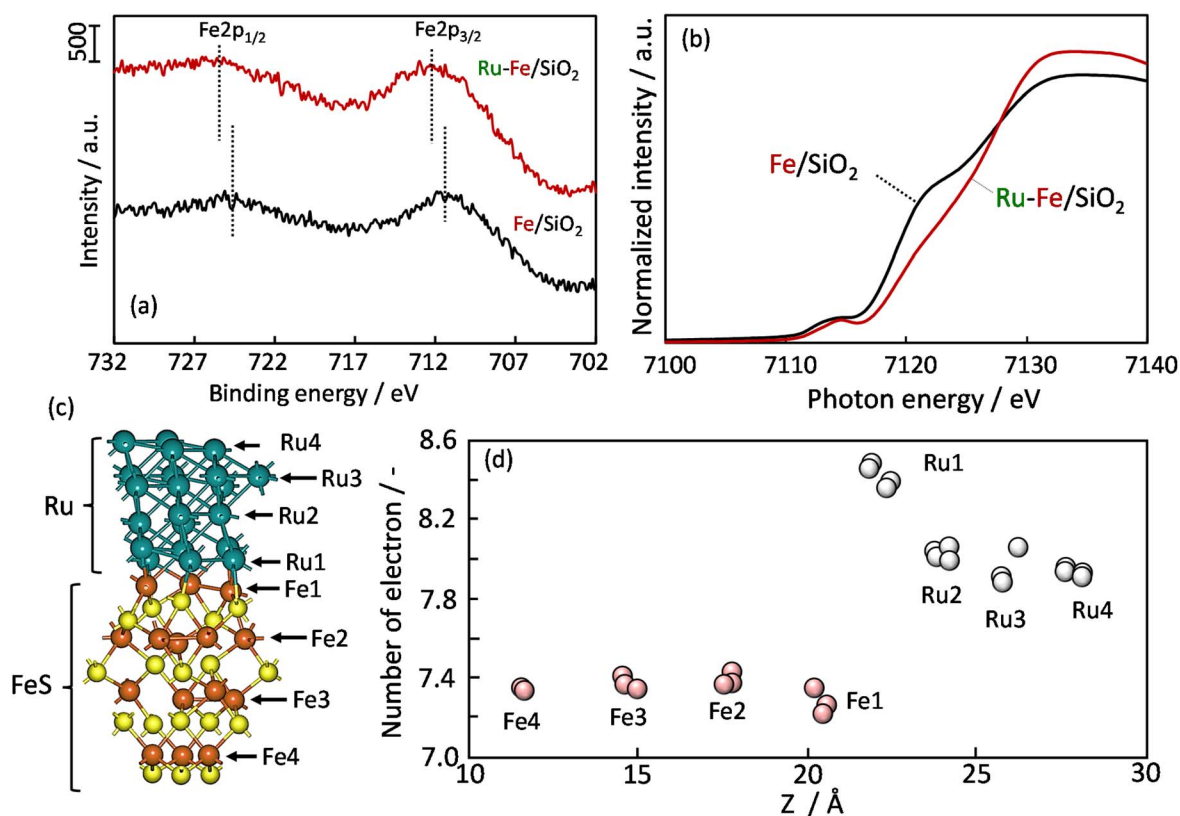

Fig. 7 (a) XPS spectra of the Fe $2p_{3/2}$ peak of the Fe/SiO2 and Ru–Fe/SiO2 catalysts. (b) Fe K-edge XANES spectra of the Fe/SiO2 and Ru–Fe/SiO2 catalysts after pre-sulphurisation. (c) Optimum structure image of interface between FeS and Ru. (d) Number of electrons of Fe and Ru in the optimum structure shown in (c).

neighboring Ru atoms (Ru_1), leading to a local oxidation of Fe and reduction of Ru at the interface. This electron redistribution supports the experimentally observed increase in Fe^{3+} content and suggests that Ru at the interface acts as a local electron acceptor. While interfacial charge transfer in such systems is mechanistically plausible, direct evidence of Ru functioning as an 'electron sink' in sulfide catalysts remains to be established. Such interfacial charge transfer is known to modulate the redox flexibility of adjacent sites and can significantly enhance lattice anion dynamics during catalytic turnover.

In summary, the combination of Ru K-edge EXAFS, XPS, and DFT analysis shows that Ru exists in dual states—metallic and sulphidic—and interacts electronically with Fe species at the catalyst interface. This dual nature enables Ru to play two cooperative roles: (1) promoting C–H bond activation through metallic Ru^0 sites, and (2) enhancing lattice S^{2-} redox cycling by oxidizing adjacent Fe sites and maintaining a more redox-flexible Fe environment. These findings rationalize the enhanced PDH activity and stability of Ru–Fe/SiO$_2$ and underscore the importance of interfacial engineering in redox-active catalysts.

4. Conclusions

In this study, we investigated the effects of noble metal promoters—Pd, Pt, and Ru—on Fe/SiO$_2$ catalysts for propane dehydrogenation under H$_2$S co-feeding. Among them, Ru provided the greatest enhancement in activity and stability, maintaining high performance even under sulfur-rich conditions. Mechanistic analysis revealed that the reaction proceeds *via* a regenerable redox cycle involving lattice S^{2-} species, which are consumed during oxidative dehydrogenation and restored by H$_2$S. Transient experiments and kinetic modeling demonstrated that Ru accelerates both sulfur release and regeneration steps, leading to a faster redox cycle. Spectroscopic and DFT analyses confirmed that Ru induces interfacial electron transfer from Fe, raising the Fe oxidation state and promoting sulfur mobility. NEB calculations further showed that all elementary steps occur within moderate and balanced energy barriers (0.62–0.84 eV), supporting the feasibility of the proposed mechanism. Overall, Ru serves as both a structural and electronic promoter, enabling a robust sulfur-mediated redox pathway for selective alkane dehydrogenation. This approach offers a new strategy for designing sulfur-tolerant, regenerable catalysts under challenging reaction environments.

Data availability

The data that support the findings of this study are available from the corresponding author, Ryo Watanabe, upon reasonable request.

Conflicts of interest

There are no conflicts to declare.

References

1 A. Corma, F. Melo, L. Sauvanaud and F. J. Ortega, *Appl. Catal., A*, 2004, **265**(2), 195–206.

2 J. Verstraete, V. Coupard, C. Thomazeau and P. Etienne, *Catal. Today*, 2005, **106**(1–4), 62–71.

3 Z. Nawaz, *Int. Rev. Chem. Eng.*, 2015, **31**(5), 413–436.

4 O. O. James, S. Mandal, N. Alele, B. Chowdhury and S. Maity, *Fuel Process. Technol.*, 2016, **149**, 239–255.

5 Z. Nawaz, *Int. Rev. Chem. Eng.*, 2015, **31**(5), 413–436.

6 Z. J. Zhao, C. C. Chiu and J. Gong, *Chem. Sci.*, 2015, **6**, 4403–4425.

7 F. Cavani, M. Koutyrev, F. Trifirò, A. Bartolini, D. Ghisletti, R. Iezzi, A. Santucci and G. Del Piero, *J. Catal.*, 1996, **158**, 236–250.

8 B. M. Weckhuysen and R. A. Schoonheydt, *Catal. Today*, 1999, **51**, 223–232.

9 R. L. Puurunen and B. M. Weckhuysen, *J. Catal.*, 2002, **210**, 418–430.

10 I. Miracca and L. Piovesan, *Catal. Today*, 1999, **52**(2–3), 259–269.

11 P. Bai, Z. Ma, T. Li, Y. Tian, Z. Zhang, Z. Zhong, W. Xing, P. Wu, X. Liu and Z. Yan, *ACS Appl. Mater. Interfaces*, 2016, **8**, 25979–25990.

12 P. Hu, W.-Z. Lang, X. Yan, L.-F. Chu and Y.-J. Guo, *J. Catal.*, 2018, **358**, 108–117.

13 B. Zheng, W. Hua, Y. Yue and Z. Gao, *J. Catal.*, 2005, **232**, 143–151.

14 S. Tan, B. Hu, W. G. Kim, S. H. Pang, J. S. Moore, Y. Liu, R. S. Dixit, J. G. Pendergast, D. S. Sholl, S. Nair and C. W. Jones, *ACS Catal.*, 2016, **6**, 5673–5683.

15 Y. Yun, J. R. Araujo, G. Melaet, J. Baek, B. S. Archanjo, M. Oh, A. P. Alivisatos and G. A. Somorjai, *Catal. Lett.*, 2017, **147**, 622–632.

16 M. Chen, J. Xu, Y. Gao, H.-Y. He, K.-N. Fan and J.-H. Zhuang, *J. Catal.*, 2010, **272**, 101–108.

17 K. Xia, W.-Z. Lang, P.-P. Li, X. Yan and Y.-J. Guo, *J. Catal.*, 2016, **338**, 104–114.

18 G. Wang, C. Li and H. Shan, *ACS Catal.*, 2014, **4**(4), 1139–1143.

19 E. Cheng, L. McCullough, H. Noh, O. Farha, J. Hupp and J. Notestein, *ACS Publications*, 2019, **59**(3), 1113–1122.

20 D. E. Resasco, B. K. Marcus, C. S. Huang and V. A. Durante, *J. Catal.*, 1994, **146**(1), 40–55.

21 G. Wang, C. Gao, X. Zhu, Y. Sun, C. Li and H. Shan, *ChemCatChem*, 2014, **6**(8), 2305–2314.

22 A. M. Arinaga, S. Liu and T. J. Marks, *Catal. Sci. Technol.*, 2020, **10**, 6840–6848.

23 M. Lorenzetti, *Oil Gas J.*, 2002, **100**(52), 30.

24 R. Watanabe, Y. Hondo, K. Mukawa and C. Fukuhara, *J. Mol. Catal. A:Chem.*, 2013, **377**, 74–84.

25 R. Watanabe, N. Hirata, Y. Yoda and C. Fukuhara, *Appl. Catal., A*, 2019, **587**, 117238.

26 R. Watanabe, H. Suganuma, Y. Yoda, F. Karasawa, P. Verma and C. Fukuhara, *Appl. Catal., A*, 2024, **683**, 119848.

27 V. V. Rozanov, *Russ. Chem. Rev.*, 1997, **66**(2), 107–119.